https://doi.org/10.5194/acp-2021-103
Preprint. Discussion started: 11 March 2021

Atmospheric Chemistry and Physics Discussions

Spatial and temporal variations of CO_2 mole fractions observed at Beijing, Xianghe and Xinglong in North China

Yang Yang[1,2,7], Minqiang Zhou[2,3,7], Ting Wang[2,7], Bo Yao[6], Pengfei Han[5], Denghui Ji[2,7], Wei Zhou[4,7], Yele Sun[4,7], Gengchen Wang[2,7], and Pucai Wang[2,7]

[1]Shanghai Ecological Forecasting and Remote Sensing Center, Shanghai, China
[2]Key Laboratory of Middle Atmosphere and Global Environment Observation (LAGEO), Institute of Atmospheric Physics, Chinese Academy of Sciences, Beijing, China
[3]Royal Belgian Institute for Space Aeronomy, Brussels, Belgium
[4]State Key Laboratory of Atmospheric Boundary Layer Physics and Atmospheric Chemistry (LAPC), Institute of Atmospheric Physics, Chinese Academy of Sciences, Beijing, China
[5]State Key Laboratory of Numerical Modeling for Atmospheric Sciences and Geophysical Fluid Dynamics (LASG), Institute of Atmospheric Physics, Chinese Academy of Sciences, Beijing, China
[6]The China Meteorological Administration, Meteorological Observation Centre
[7]University of Chinese Academy of Sciences, Beijing, China

Correspondence: Minqiang Zhou (minqiang.zhou@aeronomie.be); Ting Wang (wangting@mail.iap.ac.cn)

Abstract. Atmospheric CO_2 mole fractions are observed at Beijing (BJ), Xianghe (XH), and Xinglong (XL) in North China using the Picarro G2301 Cavity Ring-Down Spectroscopy instruments. The measurement system is described comprehensively for the first time. The geo-distances among these three sites are within 200 km, but they have very different surrounding environments: BJ is inside the megacity; XH is in the suburban area; XL is in the countryside on a mountain. The mean and standard deviation of CO_2 mole fractions at BJ, XH, and XL between October 2018 and September 2019 are 448.4±12.8 ppm, 436.0±9.2 ppm and 420.6±8.2 ppm, respectively. The seasonal variations of CO_2 at these three sites are similar, with a maximum in winter and a minimum in summer, which is dominated by the terrestrial ecosystem. However, the seasonal variations of CO_2 at BJ and XH are more affected by human activities as compared to XL. By using CO_2 at XL as the background, CO_2 enhancements are observed simultaneously at BJ and XH. The diurnal variations of CO_2 are driven by the boundary layer height, photosynthesis and human activities at BJ, XH and XL. Moreover, we address the impact of the wind on the CO_2 mole fractions at BJ and XL. This study provides an insight into the spatial and temporal variations of CO_2 mole fractions in North China.

1 Introduction

Carbon dioxide (CO_2) is the largest contributor to the total positive radiative forcing of the earth among anthropogenic gases. CO_2 has reached up to 140% relative to the pre-industrial level mainly due to fossil fuel combustion and land-use change (IPCC, 2013). The increase in CO_2 has led to an imbalance of 0.58 ±0.15 Wm^{-2} in energy budget between 2005 and 2010 at the top of atmosphere (Hansen et al., 2011), resulting into changes in the atmospheric temperature, the sea level, and the hydrology. Urban areas only take up around 2% of global land cover, while they emit more than 70% of CO_2 emissions from burning

https://doi.org/10.5194/acp-2021-103
Preprint. Discussion started: 11 March 2021


Atmospheric Chemistry and Physics Discussions

fossil fuels (Churkina, 2016). According to Gao et al. (2018), CO_2 emissions in metropolitan regions increased continuously from 1985 to 2006. Dhakal (2009) showed that China's urbanization rate has already reached 40% in 2005 and it is predicted to reach up to the level of 60% in 2030. This kind of increase certainly demands large quantities of energy consuming, leading to a large amount of CO_2 emissions.

It is important to understand atmospheric CO_2 variations in urban, suburban and rural areas. Previous studies carried out in urban areas, such as Phoenix, USA (Idso et al., 2013) and Copenhagen, Denmark (Soegaard and Møller-Jensen, 2003) show that CO_2 mole fractions are larger in the city center as compared to the outskirts, which is called "urban CO_2 dome". Various underlying surfaces, such as buildings, roads, trees, croplands, and grasslands cause complicate CO_2 characteristics (Cheng et al., 2018). George et al. (2007) pointed out that the horizontal gradients of CO_2 mole fractions among urban, suburban and rural areas are caused by different population densities and traffic volumes.

The Beijing-Tianjin-Hebei (BTH) area is an economically dynamic region, located in North China, with highly urbanized cities, suburban cities and rural areas (Figure 1). During the last two decades, the population in Beijing has increased from 13.64 million in 2000 to 21.54 million in 2018, the car amount increases from 1.04 million in 2000 to 5.74 million in 2018 (http:/data.stats.gov.cn/). In the BTH area, the major CO_2 emissions are coming from industry, residential emissions, power plant and transportation (Song et al., 2013; Feng et al., 2019). In order to reduce the carbon emissions, Beijing has adopted a number of vehicle emission control strategies since the mid-1990s, for example, emission control on new and in-use vehicles, fuel quality improvements, alternative-fuel and advanced vehicles and public transport (Wu et al., 2011). During the China's 12th (2011-2015) and 13th (2016-2020) Five-Year Plan periods, comprehensive work programs have been implemented for energy conservation and emission reduction in Beijing. More recently, Beijing has also launched the short-term 'the three-year blue-sky defense battle of Beijing' between 2018 and 2020. Regional networks incorporated with high-accuracy CO_2 measurements can be used to retrieve carbon emissions and sinks in the horizontal gradient. The vertical gradient of CO_2 mole fractions can also be observed at several different heights at the same location (Bakwin et al., 1998).

To better understand the characteristics of CO_2 variations in the BTH area, 3 Cavity Ring-down Spectroscopy (CRDS) analyzers (Picarro G2301) within 200 km were installed at Beijing (BJ), Xianghe (XH), and Xinglong (XL). The three sites have very different surrounding environments: BJ is inside the megacity, XH is in the suburban area, and XL is in the countryside on a mountain. The measurements between June 2018 and April 2020 at the three sites allow us to better understand the differences among the urban, suburban and rural sites about the seasonal, synoptic and diurnal variations of CO_2 mole fractions. Section 2 describes the site locations as well as the measurement system. The results and discussions are presented in Section 3. Finally, the conclusions are drawn in Section 4.

2 Measurements

2.1 Sites

The locations of the three sites at BJ (39.96 °N, 116.36 °E, 49 m above sea level (a.s.l.)), XH (39.75 °N, 116.96 °E, 30 m a.s.l.) and XL (40.40°N, 117.50 °E, 940 m a.s.l.) are shown in Figure 1. The red bars above the sites are the anthropogenic carbon

https://doi.org/10.5194/acp-2021-103
Preprint. Discussion started: 11 March 2021

Atmospheric Chemistry and Physics Discussions

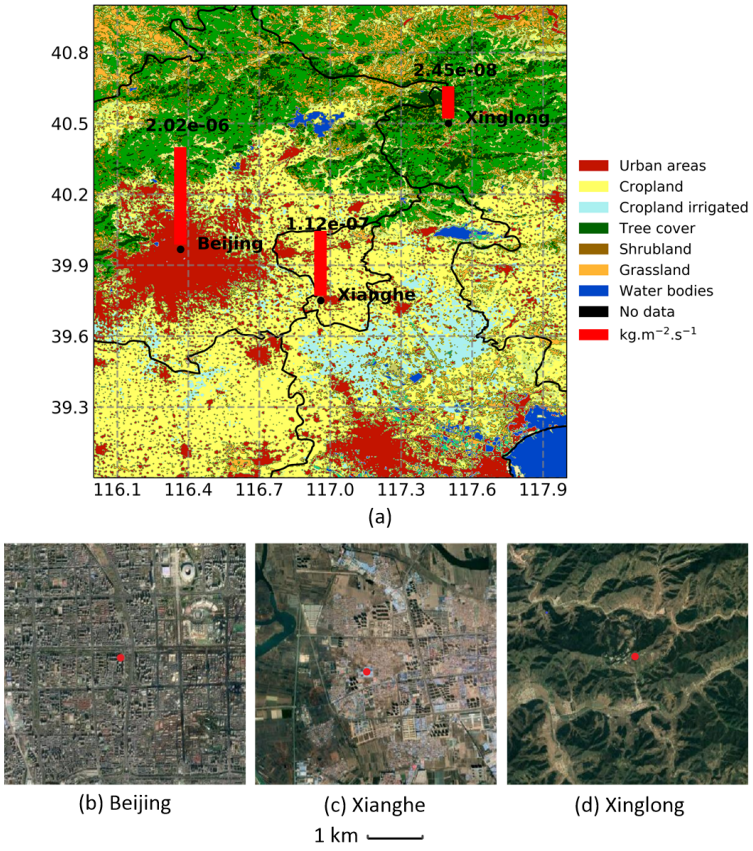

Figure 1. (a): the Location of three sites at Beijing (BJ, 39.96 °N, 116.36 °E, 49 m a.s.l.), Xianghe (XH, 39.75 °N, 116.96 °E, 30 m a.s.l.) and Xinglong (XL, 40.40°N, 117.50 °E, 940 m a.s.l.), together with the land cover in this area. The red bars are the carbon dioxide emissions at the 3 sites based on the EDGAR data. The map within ~2 km of BJ (b), XH (c) and XL (c) are coming from © Google Maps (https://www.google.com/maps).

dioxide emissions in 2015 from the Emission Database for Global Atmospheric Research (EDGAR) v5.0 (Crippa et al., 2019). The CO_2 fluxes are 2.02×10^{-6}, 1.12×10^{-7}, and 2.45×10^{-8} kg m^{-2} s^{-1} at BJ, XH and XL, respectively.

The BJ site is located in a highly urbanized area, with dense buildings, shopping centers, roads and residential districts. To the east of the site, there is the Beijing-Tibet expressway (G6) carrying a heavy volume of traffic. Within 1 km of the site, the heights of trees are about 15-20 m, and the heights of buildings are about 70-200 m (Cheng et al., 2018). The vegetation fractions around the BJ site are between 10% and 18% (Liu et al., 2012).

The XH site is in a suburban area about 50 km to the southeast of Beijing. XH is surrounded by croplands and irrigated croplands. Within 1 km of the XH site, the residential houses are mainly home-built, with an average height of ~20 m. The center of Xianghe county is about 2 km to the east of the site.

https://doi.org/10.5194/acp-2021-103
Preprint. Discussion started: 11 March 2021

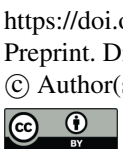

Atmospheric Chemistry and Physics Discussions

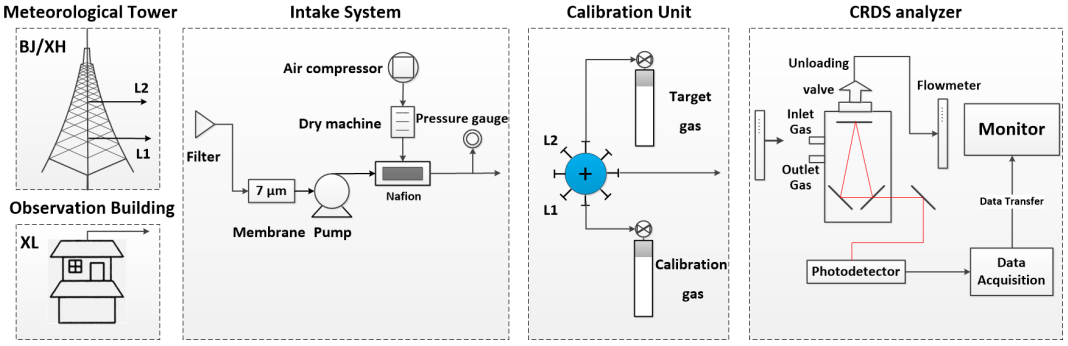

Figure 2. The schematic diagram of measurement system, including a meteorological tower at BJ/XH or observation building at XL, an intake system, a calibration unit and a CRDS analyzer.

The XL site is located on a mountain, inside the Xinglong Observatory of the National Astronomical Observatories, Chinese Academy of Sciences (NAOC) (https://www.xinglong-naoc.org/html/en/), which is about 120 km to the northeast of Beijing. XL is located in a highly vegetated area.

2.2 Instrumentation

The Picarro Cavity Ring-Down Spectroscopy (CRDS) G2301 analyzers were installed at BJ, XH, and XL to measure CO_2, CH_4, and H_2O mole fractions. The same measurement system is operated at these three sites, which is composed of an intake system, a calibration unit, and a Picarro analyzer (Figure 2). Note that there are two sampling heights at BJ (80 and 280 m above ground level (a.g.l.)) and XH (60 and 80 m a.g.l.), but only one sampling height (10 m a.g.l.) at XL. The measurements start in June 2018 at BJ and XH, and in May 2016 at XL. To compare the CO_2 measurements among these sites, we focus on the data after June 2018 in this study.

2.2.1 Intake system

The surrounding air is sampled by a vacuum pump (DA7002D) with a maximum flux of 20 L.min^{-1} through an inlet. The sample air is then introduced into a 10 mm-diameter tube (SYNFLEX 1300), mounted with a capsule filter (Whatman, USA) to filter out the solid particle with a diameter larger than 2 μm and liquid particles with a diameter larger than 0.03 mm. In addition, a 7 mm sintered filter (Membrane) is installed to filter out the solid particle with a diameter larger than 7 μm. Moreover, an air compressor and a dry machine together with a single Nafion tubing selectively permeable membrane dryer (MD-110-72P-4; Perma Pure, Halma, UK) in self-purge are installed to remove water vapor. The sample dew-point temperature can reach down to -25 °C, corresponding to a relative humidity of 1-20 %. The flux of the Nafion outflow is 200-400 ml min^{-1}. The outflow is then vented to the unloading valve (Figure 2), which guarantees that the air fed to the Picarro G2301 analyzer is controlled at near-ambient pressure.

https://doi.org/10.5194/acp-2021-103
Preprint. Discussion started: 11 March 2021


Atmospheric Chemistry and Physics Discussions

2.2.2 Calibration unit

The intake system is connected to an 8-position valve, which is used to choose the air coming from the sample air, the target gas, or the calibration gas. The target and calibration gases are pressurized in 29.5 L treated aluminum alloy cylinders, which are scaled to the WMO X2007 standard by the China Meteorological Administration, Meteorological Observation Centre. The same calibration procedure is operated at these three sites: 1) 3-hours sample air; 2) 5-minutes calibration gas; 3) 3-hours sample air; 4) 5-minutes target gas. This process repeats every 6 hours and 10 minutes. Note that, the airs coming from two levels at XH and BJ are switched every 5 minutes during the 3-hours sample air period. As the remaining volume in the tubes needs time for flushing, the response of the analyzer turns to be stable about 1 minute after each switching. In order to reduce the uncertainty, we do not consider the first 3-minutes measurements after each switching.

The calibration gas is to calculate the calibration factor (cf),

$$cf = \overline{CO_{2,mcal}/CO_{2,cal}}, \tag{1}$$

where $CO_{2,mcal}$ is the CO_2 mole fraction measured by the Picarro analyzer from the calibration gas and $CO_{2,cal}$ is the standard CO_2 mole fraction of the calibration cylinder. cf is applied to correct the sample air during the next 6 hours,

$$CO_{2,c} = cf \times CO_{2,m}, \tag{2}$$

where $CO_{2,m}$ is the CO_2 mole fraction measured by the Picarro analyzer and $CO_{2,c}$ is the calibrated CO_2 mole fraction.

The target gas is used to check the precision and stability of the system. The T value are calculated as follows,

$$T = cf \times CO_{2,mtar} - CO_{2,tar}, \tag{3}$$

where $CO_{2,tar}$ is the standard CO_2 mole fraction of the target gas cylinder, $CO_{2,mtar}$ is the CO_2 mole fraction measured by the Picarro analyzer from the target gas. In this study, we only select the period with T value within $\pm$ 0.1 ppm (Fang et al., 2014). The measurement uncertainties of the Picarro instrument at the three sites are calculated as the standard deviation (std) of T, which are 0.01, 0.06, and 0.02 ppm at BJ, XH, and XL respectively. What's more, to reduce the uncertainties of the inlet filter, pump, and extreme weather, we manually flag and filter out the abnormal CO_2 measurements at these three sites.

2.2.3 Picarro analyzer

The Picarro analyzer is composed of a laser, a high-finesse optical cavity, and a detector. The sample air is first introduced into the cavity. After that, the laser passes through the sample air and the intensity of the laser arriving at the detector is monitored as I. Then, the 'ring-down' measurements start as the laser rapidly shuts down. Meanwhile, the sample gas is measured by recording the decay of the laser intensity with time. This decay depends on the optical path inside of the cavity, which is in correlation with the absorption and scattering of the sample air. The analyzer continuously scans the laser over CO_2 spectral features and records the absorption loss at a wavelength of 1603 nm to form the spectrum. As a result, CO_2 mole fractions are derived from these spectra and collected by the Data Acquisition part. The temporal resolution of the CO_2 measurements is 2 seconds.

https://doi.org/10.5194/acp-2021-103
Preprint. Discussion started: 11 March 2021

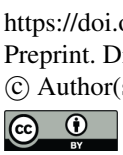

Atmospheric Chemistry and Physics Discussions

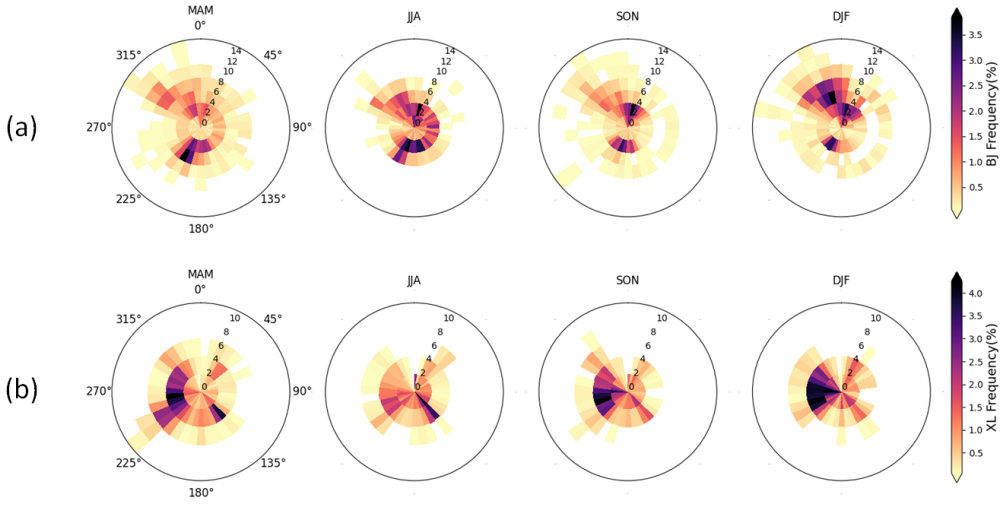

Figure 3. Wind frequency as a function of wind speed (m.s^{-1}) and wind direction (°) in each season at BJ (a) and XL (b) from October 2018 to September 2019.

2.3 Meteorological fields

The CO_2 variations are additionally characterized by specific meteorological parameters, such as local wind and temperature fields. The local meteorological sensors at BJ are installed at the same tower as the Picarro on 120 m a.g.l., and the meteorological sensors at XL are ~5 m northwest to the Picarro sample tube. The meteorological fields at XH are not discussed here as there is a technical issue with the wind sensor.

Figure 3 shows the wind frequencies at BJ and XL in each season, which are binned with a resolution of 2 m.s^{-1} for the wind speed and 10°for the wind direction. At BJ, two dominant wind regimes are observed throughout the whole year: north (northwest to northeast clockwise) and southwest. The percentage of wind frequency in the north region is 34%, 36%, 50% and 60% respectively from spring to winter. The wind speed varies from 0.63 m.s^{-1} on 10 May 2019 to 14.98 m.s^{-1} on 20 December 2018, with a mean of 3.92 m.s^{-1}. From spring to autumn, more winds are with a low wind speed. However, in winter, the prevailing northwest wind contributes to high wind frequencies with the increase of wind speed. At XL, the dominant winds are mainly from the west (southwest to northwest clockwise), together with some winds from the southeast. The percentage of wind frequency in the west region is 52%, 33%, 56% and 57% respectively from spring to winter. The wind speed varies from near-zero on 18 August 2019 to 10.75 m.s^{-1} on 17 April 2019, with a mean of 2.52 m.s^{-1}.

The atmospheric boundary layer height (BLH) is an important parameter to characterize the diurnal variation of CO_2 (Li et al., 2014; Culf et al., 1997). In this study, we use the BLH hourly data of the ERA5 reanalysis data from the European Centre for Medium-Range Weather Forecasts (ECMWF) with a spatial resolution of 0.25 °× 0.25 °(Hersbach et al., 2020).

https://doi.org/10.5194/acp-2021-103
Preprint. Discussion started: 11 March 2021

Atmospheric Chemistry and Physics Discussions

3 Results and discussions

3.1 CO_2 time series

Figure 3 shows the time series of hourly CO_2 mole fractions at the three sites between June 2018 and March 2020. The two-levels (80 m and 280 m) measurements at BJ are marked as BJ L1 and BJ L2, and the two-levels (60 m and 80 m) measurements at XH are marked as XH L1 and XH L2. The gaps in the CO_2 time series are due to the malfunctions of the instruments. To better understand the influence of the wind on CO_2, we classify the CO_2 mole fractions at XL and BJ L1 based on the wind information into five classes respectively (Fig. 4a and b). The BJ L1 is used here as it is closer to the wind sensor as compared to BJ L2. The local class is defined as wind speed less than 2 m.s^{-1}, while the wind speed larger than 2 m.s^{-1} are classified into four sections according to the wind direction: northwest (NW), northeast (NE), southwest (SW) and southeast (SE).

As expected, the urban BJ site observes a much higher CO_2 level than the suburban XH and rural XL sites. The CO_2 measurements at the urban site BJ L1 (Fig. 4b) are influenced by the wind speeds and wind directions. High CO_2 mole fractions generally appear in local class throughout the whole year, indicating the strong local anthropogenic emissions. The north sectors (NS and NE) usually contribute low CO_2 mole fractions during the autumn-winter period. However, in spring and summer, the SW sector contributes lower CO_2, indicating the low CO_2 varies with the wind direction season by season at BJ. Different from BJ, the CO_2 mole fraction in the local class at XL covers all the data range throughout the whole year. In spring and summer, the wind from the south (SE and SW) makes CO_2 increase at XL.

As XL is located in a rural area that is less influenced by human activities as compared to BJ and XH, we take CO_2 at XL as the background. The CO_2 enhancement at BJ or XH relative to XL is then calculated as

$$\Delta CO_{2,BJ/XH} = CO_{2,BJ/XH} - CO_{2,XL} \quad (4)$$

The time series of hourly Δ $CO_{2,BJ/XH}$ are presented in Figure 5a. The Δ CO_2 has a maximum in winter and a minimum in summer at both BJ and XH. The high value is probably related to more combustion of fossil fuel from traffic and heating systems in winter (Liu et al., 2012). The daily Δ CO_2 can reach up to 106.8 ppm in December 2018 at BJ and 78.5 ppm in January 2019 at XH. The mean Δ CO_2 at BJ and XH are 26.2 ppm and 15.2 ppm, respectively.

There are 271 days when Δ CO_2 are observed at both BJ and XH (Figure 5b). The correlation efficiency (R) of 0.81 is found between the Δ CO_2 at BJ and XH, indicating that the Δ CO_2s change simultaneously at BJ and XH. The slope of the linear fitting suggests that the Δ CO_2 at BJ is 1.23 times larger than that of XH.

3.2 Seasonal variations

The seasonal cycles of CO_2 are derived from the measurements at the lower levels at BJ and XH, and the measurements at XL. The lower levels at BJ and XH are used here as they reflect more information about surface fluxes. Figure 6a shows the CO_2 monthly means between October 2018 and September 2019, together with the temperature at BJ and leaf area index (LAI). The LAI monthly data are from the Copernicus Global Land Service (https://land.copernicus.eu/global/products/lai) with a spatial resolution of 1 km. Figure 6a shows the LAI monthly means in the region of Fig. 1.

https://doi.org/10.5194/acp-2021-103
Preprint. Discussion started: 11 March 2021

Atmospheric Chemistry and Physics Discussions

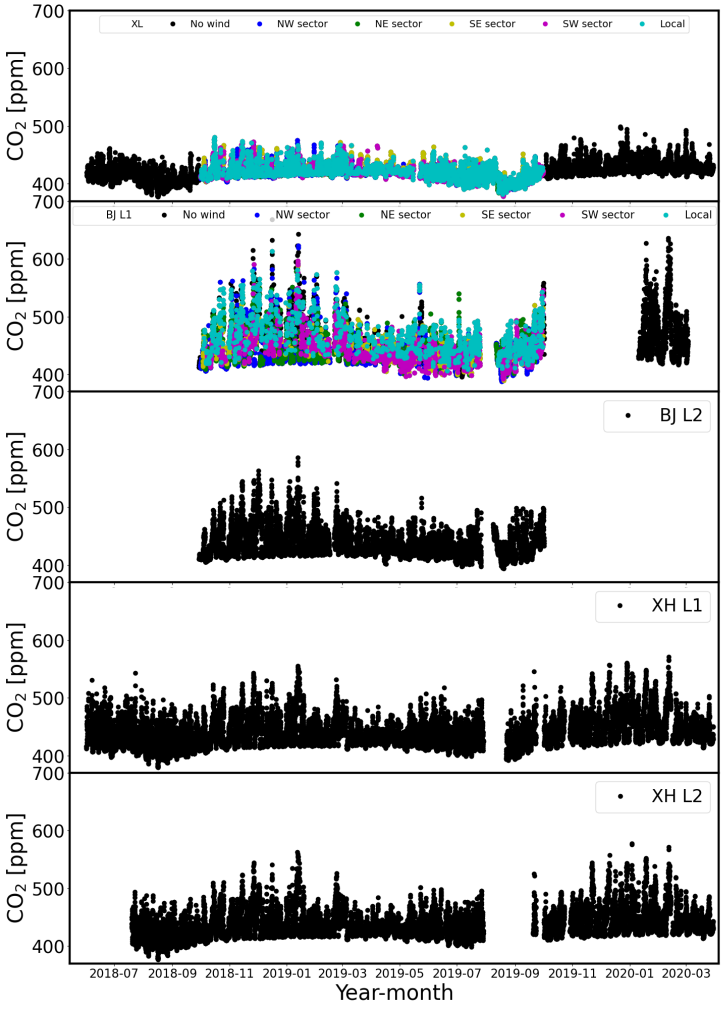

Figure 4. The time series of the CO_2 measurements at XL (a), BJ L1 (b), BJ L2 (c), XH L1 (d) and XH L2 (e) between June 2018 and March 2020. The CO_2 measurements at XL (a) and BJ LI (b) are colored by wind classes discussed in the text.

https://doi.org/10.5194/acp-2021-103
Preprint. Discussion started: 11 March 2021

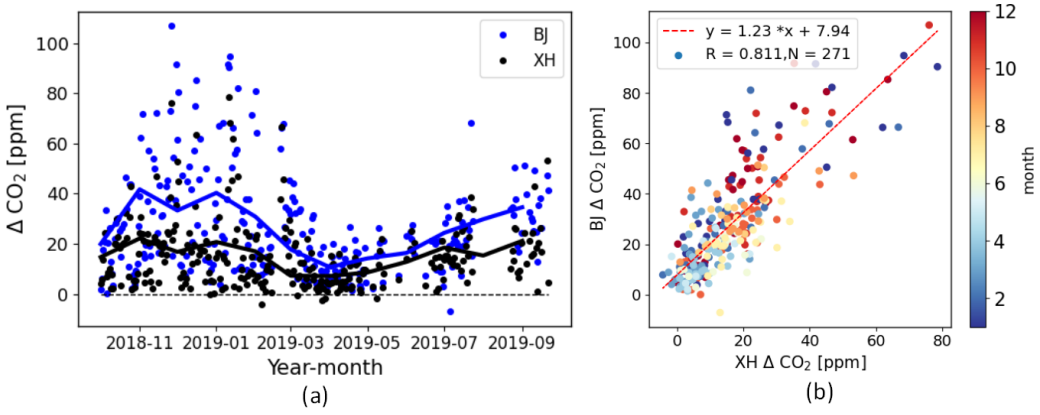

Figure 5. (a): the time series of daily CO_2 enhancements at BJ and XH relative to XL between October 2018 and September 2019. The blue and black lines are the monthly means of CO_2 enhancements at BJ and XH, respectively. (b): the correlation between daily mean CO_2 enhancements at BJ and XH.

Between October 2018 and September 2019, the mean of CO_2 mole fractions at BJ is 448.4±12.8 ppm, which is larger than those at XH (436.0±9.2 ppm) and XL (420.6±8.2 ppm). The phases of the seasonal cycle of CO_2 at BJ, XH and XL are similar, with a high value in autumn-winter and a low value in summer, which is consistent with other observations in North Hemisphere (Nevison et al., 2008). It is expected mainly due to the seasonal cycle of the biosphere fluxes (LAI). The increased temperature in summer is favorable for plant growth, leading to larger photosynthesis. In winter, the respiration of plants and the anthropogenic heating emissions contribute to a high CO_2 level. The amplitudes of the seasonal variation of CO_2 at BJ, XH and XL are 60.3 ppm, 36.1 ppm and 29.3 ppm, respectively.

Figure 6b, c and d show the CO_2 monthly means together with the monthly 1σ standard deviation at each site. We take the days when measurements are available at all three sites or the days when measurements are available at XH and XL. The CO_2 variability (1σ) is highest at BJ and lowest at XL. The seasonal CO_2 variation and 1σ standard deviation at each site are further assessed in the following.

Autumn. At each site, monthly mean CO_2 mole fractions are increasing with the decrease of LAI. The increase rates of CO_2 at BJ, XH and XL are 30, 19 and 9 ppm/month, respectively. The 1σ standard deviation of each month at BJ is generally larger than that of XH, then followed by XL.

Winter. The CO_2 removed by the photosynthesis is weak in this region as the LAI is low. The CO_2 change simultaneously at BJ and XH, increasing from December 2018 to January 2019 and decreasing afterwards. Similar to autumn, the month-to-month variation of CO_2 at BJ is larger than those at BJ and XL, together with the largest 1σ at BJ. The 1σ at BJ and XH is larger in winter as compared to other seasons.

Spring. The decrease of CO_2 in March 2019 is highly related to the temperature increase. As the heating is officially stopped in the middle of March, the anthropogenic emissions are much reduced (Shi et al., 2020). In April and May, the LAI increases

https://doi.org/10.5194/acp-2021-103
Preprint. Discussion started: 11 March 2021

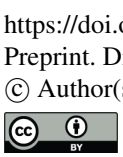

Atmospheric Chemistry and Physics Discussions

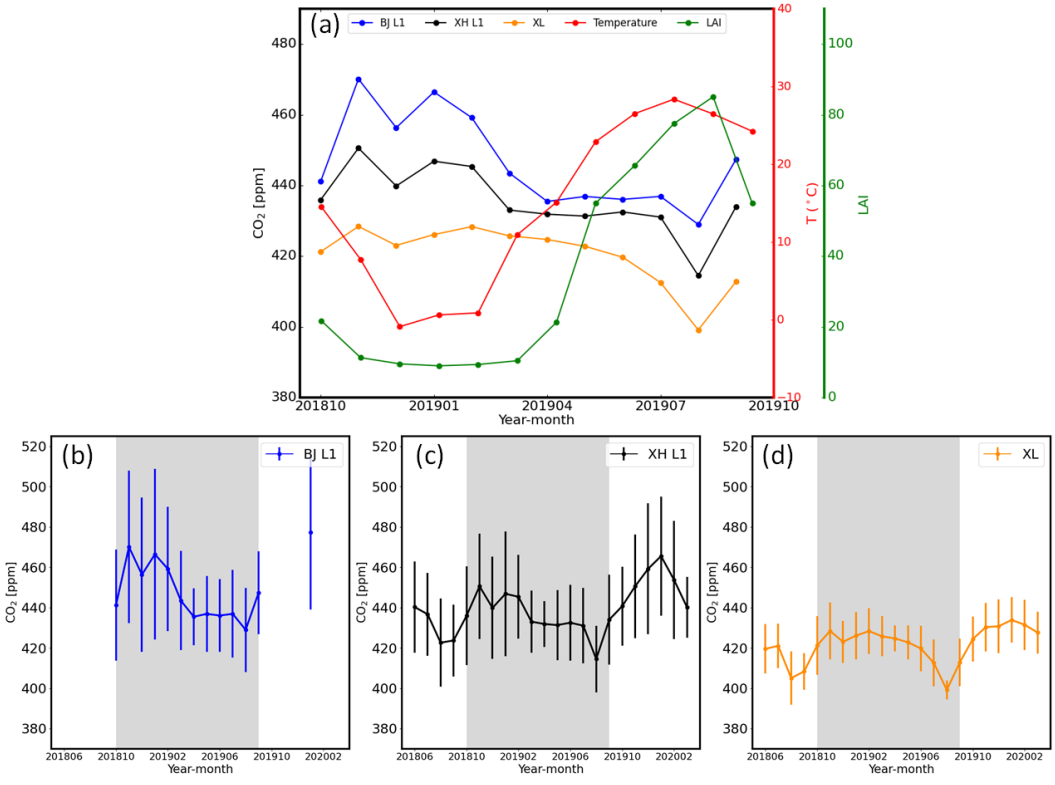

Figure 6. (a): the monthly means of CO_2 at BJ L1, XH L1 and XL between October 2018 and September 2019. The monthly mean air temperature at BJ and regional mean Leaf Area Index (LAI) of the area in Figure 1a during the same period are also displayed. (b-d): monthly means of CO_2 together with the 1σ standard deviation at BJ L1, XH L1 and XL between June 2018 and February 2020. The gap at BJ L1 is due to the instrument failure. The shadow is the measurement period displayed in Figure 6a.

significantly, leading to the decrease of CO_2, especially at XL. The regional biosphere activity affects more on CO_2 mole fractions at XL, while the large anthropogenic emissions at BJ and XH may reduce the influence from the photosynthesis.

Summer. At all the sites, the minimum CO_2 is observed in August with the maximum LAI corresponding to the largest photosynthesis CO_2 absorption activity. The month-to-month variation of 1σ is small at BJ and XH.

3.3 Diurnal variations

The diurnal variations of CO_2 at BJ, XH and XL between October 2018 and September 2019 are shown in Figure 7. The amplitudes of the diurnal variations are between 16.4 ppm and 44.1 ppm at BJ. The relatively large amplitudes are observed in summer and winter compared to spring and autumn. The phase of the diurnal variation at BJ varies with season. There are one peak in the early morning (4:00-7:00) and one trough in the afternoon (14:00-16:00) in spring and summer. However, there are two peaks (8:00-9:00, 22:00-1:00), and two troughs (4:00-7:00, 14:00-16:00) in late autumn and winter. At XH, there are

https://doi.org/10.5194/acp-2021-103
Preprint. Discussion started: 11 March 2021

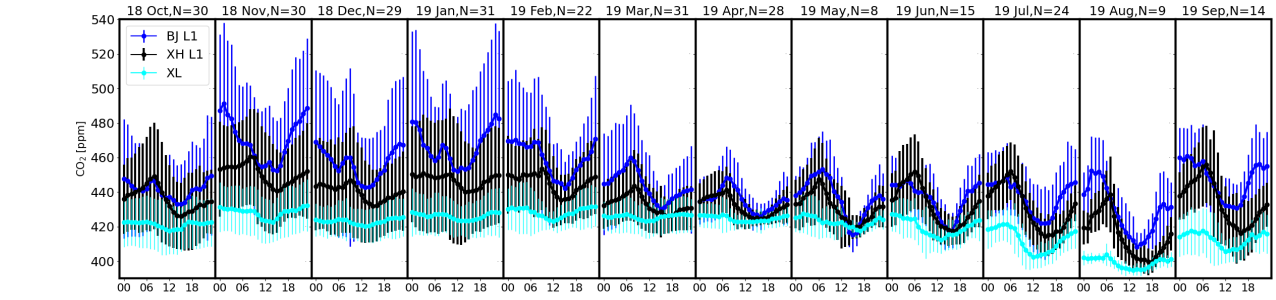

Figure 7. The diurnal cycles of CO_2 variations at BJ L1, XH L1 and XL in each month between October 2018 and September 2019. The collocated days are displayed (N). The error bars are the hourly standard deviations of CO_2.

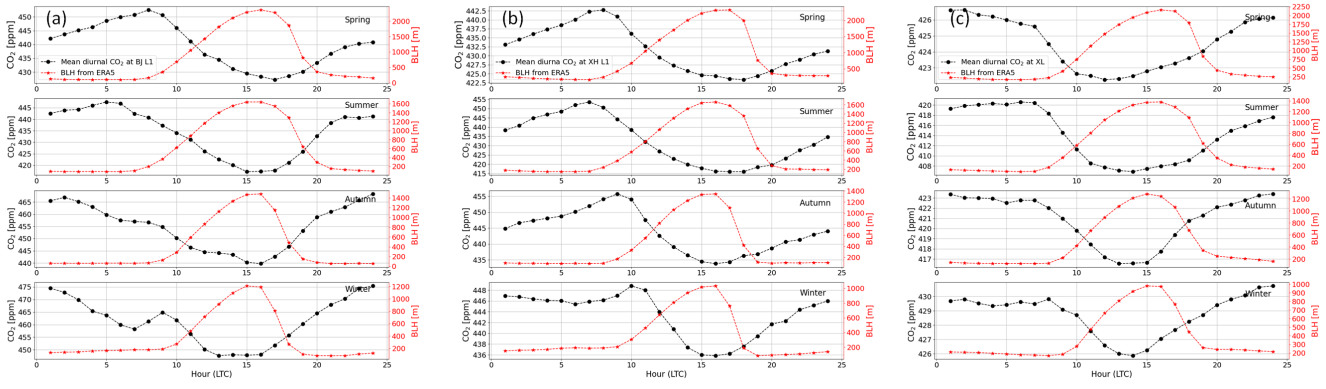

Figure 8. (a-c): mean diurnal cycles of BLH from ERA5 and mean diurnal CO_2 variations at BJ L1 (a), XH L1 (b) and XL (c) in each season between October 2018 and September 2019.

one peak (4:00-7:00) and one trough (14:00-16:00) throughout the whole year. The amplitude of the diurnal variation at XH is about 6-20 ppm smaller than that at BJ between November 2018 and May 2019. At XL, the peak of CO_2 occurs around 4:00-7:00, and the trough occurs in the afternoon around 12:00-14:00. The amplitudes of diurnal variations at XL are larger in summer as compared to other seasons. Moreover, the amplitudes of diurnal variations at XL are much smaller as compared to those at BJ and XH, especially in winter.

The diurnal variations of CO_2 are mainly affected by the BLH, photosynthesis, and local human activities (Chan et al., 2008; Denning et al., 1999). Generally, the increase of sunlight enhances the plant photosynthetic rate, vice versa. There is no photosynthetic CO_2 sink before sunrise or after sunset (Lv et al., 2020; Bagley et al., 2015). To better understand the influence of the BLH on the diurnal CO_2 variations, we show the CO_2 diurnal cycles for each season at BJ L1, XH L1 and XL, together with the BLH hourly means.

https://doi.org/10.5194/acp-2021-103
Preprint. Discussion started: 11 March 2021


Atmospheric Chemistry and Physics Discussions

BJ L1. The increase of the BLH after sunrise (5:00 - 8:00) and the photosynthetic uptake during the day make the CO_2 mole fraction decrease. The CO_2 mole fraction reaches a minimum in the afternoon around 16:00-17:00, corresponding to the maximum BLH. After that, the BLH decreases resulting into the accumulation of CO_2. In spring and summer, the CO_2 mole fraction keeps increasing until the next day (5:00-8:00) before sunrise, and in autumn and winter, the CO_2 mole fraction starts decreasing at midnight. Note that the enhancement of CO_2 around 9:00 in winter is not related to the BLH, which is probably due to the rush traffic emission.

XH L1. Similar to BJ, the variation of the CO_2 mole fraction is dominated by the BLH during the day. The CO_2 mole fraction decreases with the increase of BLH. The CO_2 mole fraction reaches a minimum in the afternoon around 16:00-17:00, corresponding to the highest BLH. However, at night, the variation of CO_2 at XH is not the same as that at BJ, especially in autumn and winter. In autumn, the CO_2 mole fraction keeps increasing until next day before sunrise (5:00-8:00), and in winter, the CO_2 mole fraction stays stable after midnight. Similar to BJ, the peak CO_2 around 9:00-10:00 in winter may be due to the traffic emission in the rush hour.

XL. Different from BJ and XH, the minimum of the CO_2 mole fraction occurs earlier than the maximum of BLH in spring and summer. For example, the minimum of the CO_2 mole fraction is around 12:00 and the maximum of BLH occurs around 16:00. The solar radiation is strongest at noon, which leads to the largest photosynthesis removing CO_2. The diurnal variation of CO_2 at daytime is then strongly affected by the plants in these two seasons. However, in autumn and winter, the minimum of the CO_2 mole fraction occurs close to the maximum of the BLH, which is probably due to the low LAI in these two seasons.

3.4 CO_2 variations with the wind

Wind speed and wind direction are the two key factors in modulating the dispersion of CO_2 emissions (Turnbull et al., 2015; Lac et al., 2013; ángeles García et al., 2012). The influence of wind on CO_2 mole fraction at BJ and XL is discussed specifically in this section. To minimize the influence from the diurnal variation, we focus on the measurements between 14:00 and 16:00 during daytime for the highest BLH, and between 22:00 and 02:00 during nighttime for the lowest BLH. Besides, we reduce the impact from the seasonal variation of CO_2 by applying the following method. First, we calculate the mean of CO_2 over 10 days ($CO_{2,10d}$). Second, the ratio between the $CO_{2,10d}$ and the annual mean of original CO_2 is derived ($Index_{10d} = CO_{2,10d}/CO_{2,mean}$), and the $Index_h$ is interpolated from the $Index_{10d}$ at an hourly scale. Finally, The deseasonalized CO_2 is calculated as $CO_{2,de} = CO_2/Index_h$. In summary, we use the deseasonalized CO_2 during the daytime (14:00-16:00) and the nighttime (22:00-02:00) separately to understand the influence of the wind.

Figure 9 shows the daytime and nighttime wind roses of CO_2 mole fractions at BJ and XL, with a resolution of 1 m.s^{-1} wind speed and of 10 °wind direction. Note that only the bins with the measurement number larger than 3 at BJ or 5 at XL are shown here.

BJ. At BJ, the wind mainly comes from the southwest and the northwest, with more winds come from the southwest during the day and more winds come from the northwest at night. The high CO_2 mole fractions are observed with a low wind speed (<2 m.s^{-1}). For the wind with a relatively large speed (>2 m.s^{-1}), it is found that the CO_2 with the wind coming from the southwest is about ~21 ppm larger than those with the wind coming from the northwest during the day.

https://doi.org/10.5194/acp-2021-103
Preprint. Discussion started: 11 March 2021


Atmospheric Chemistry and Physics Discussions

XL. The wind speed at XL is generally smaller as compared to BJ. The wind at XL is mainly coming from the southeast-northwest sector in a clockwise direction. During the day, the high CO_2 mole fractions are observed along with a relatively large wind speed (>2 m.s^{-1}). This can be attributed to the impact of remote emissions advocated from the south, where large cities, such as Beijing and Tianjin, are located. At night, although the dominant wind shifts to the west, the high CO_2 mole fractions can be observed in almost all the directions with wind speeds ranging from 0 to 3 m.s^{-1}.

3.5 Two-levels measurements at BJ and XH

Figure 10 shows the CO_2 hourly means observed at two levels at BJ and XH between October 2018 and September 2019. Note that, we select measurements when the hourly means are available at both levels. At BJ, CO_2 mole fractions at L1 are generally higher than L2, but the CO_2 mole fractions at L1 are lower than that at L2 occasionally in the afternoon in August and September 2019. The diurnal variations of CO_2 at L1 and L2 are similar in spring and summer, but not in autumn and winter. At XH, the CO_2 mole fraction at L1 is slightly larger than that at L2, especially at night. The diurnal variations at two levels at XH are close to each other, which is due to the fact that the difference in the altitudes between the two levels at XH is only 20 m.

To compare the vertical distribution of CO_2 at BJ and XH, we calculate the CO_2 gradient ($\delta CO_2 = \frac{CO_{2,L1} - CO_{2,L2}}{Alt_{L2} - Alt_{L1}}$) (Figure 10c), The diurnal variations of δCO_2 at BJ and XH have a similar pattern: close-zero during the day and positive at night. The maximum δCO_2 can reach to 0.6 ppm/m at XH in 2018 August and 0.2 ppm/m at BJ in 2018 November. The larger height difference at BJ (120 m) as compared to XH (20 m) may contribute to the smaller δCO_2.

3.6 Weekday-weekend variation

Figure 11 shows the hourly means and stds of the deseasonalized CO_2 mole fractions at BJ, XH and XL on weekdays and weekends. There is no clear difference in the CO_2 mole fraction between weekdays and weekends. However, we find that the CO_2 mole fractions have a minimum on Tuesday at BJ and XH. It is indicated that the anthropogenic emission is lowest on Tuesday. The weekday-weekend variations at BJ and XH are different from that at Nanjing China (Gao et al., 2018), where CO_2 mole fractions are higher on weekends, or from Boston USA, London UK and Tamil Nadu India, where the CO_2 mole fractions are higher on weekdays (Hernández-Paniagua et al., 2015; Kumar and Nagendra, 2015; Briber et al., 2013).

4 Conclusion

In this study, we show the CO_2 measurements from the in situ Picarro instruments at BJ, XH, and XL between June 2018 and March 2020. It is the first time to investigate CO_2 variations at these sites. BJ is inside the megacity, XH is in the suburban area, and XL is in the countryside on a mountain. The uncertainties of the CO_2 are 0.01, 0.06 and 0.02 ppm at BJ, XH and XL, respectively. The means and stds of CO_2 mole fractions are 448.4±12.8 ppm, 436.0±9.2 ppm and 420.6±8.2 ppm at BJ (L1), XH (L1) and XL, respectively. The CO_2 measurements at XL are used to represent the background and we find that there is

https://doi.org/10.5194/acp-2021-103
Preprint. Discussion started: 11 March 2021

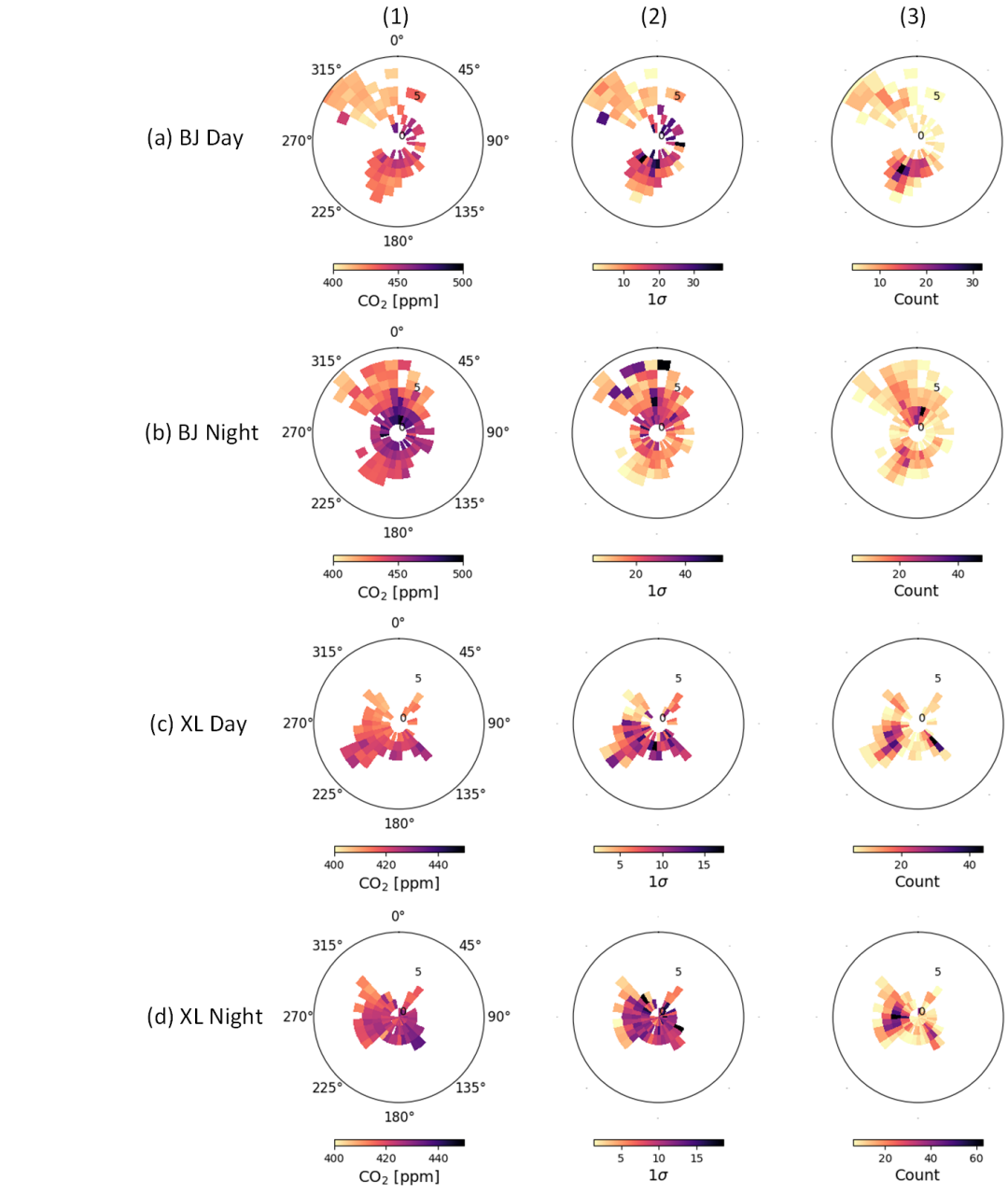

Figure 9. (1): binned CO_2 mole fraction as a function of wind speed ($m.s^{-1}$) and wind direction (°) at BJ L1 (a, b) and XL (c, d) based on daytime (14:00-16:00 LTC) and nighttime (22:00 -1:00 LTC) data between October 2018 and September 2019. (2): mean 1σ standard deviation of the CO_2 mole fractions in each bin. (3): the CO_2 measurement counts in each bin.

https://doi.org/10.5194/acp-2021-103
Preprint. Discussion started: 11 March 2021

Atmospheric Chemistry and Physics Discussions

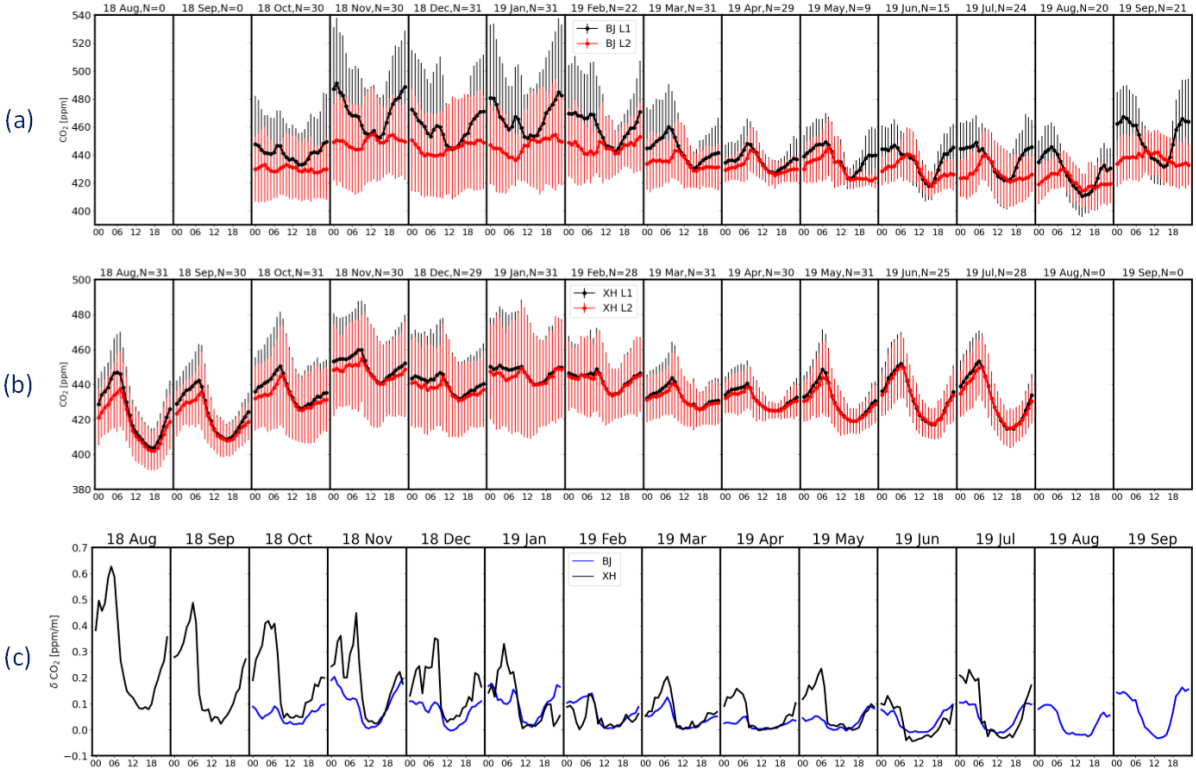

Figure 10. (a): the CO_2 measurements of BJ L1 and BJ L2 between October 2018 and September 2019. The error bars are the hourly standard deviations of CO_2. (b): the CO_2 measurements of XH L1 and XH L2 between August 2018 and July 2019. (c): the hourly δ CO_2 [ppm/m] in each month at BJ and XH.

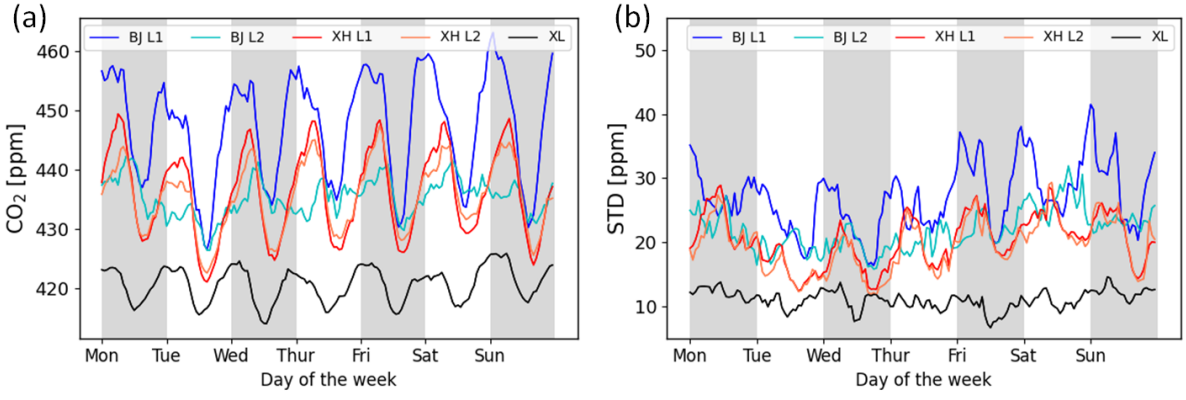

Figure 11. The hourly means (a) and standard deviations (b) of CO_2 on weekdays and weekends at BJ L1, BJ L2, XH L1, XH L2 and XL between October 2018 and September 2019.

https://doi.org/10.5194/acp-2021-103
Preprint. Discussion started: 11 March 2021


Atmospheric Chemistry and Physics Discussions

a good relationship between the CO_2 enhancements at BJ and XH. BJ and XH are affected by CO_2 emissions and transports simultaneously.

The variations of CO_2 at BJ, XH, and XL are discussed on diurnal and seasonal scales. It is found that the seasonal cycles of CO_2 at these three sites are similar, with a high value in winter and a low value in summer, which is closely related to air temperature and LAI. However, the amplitudes of seasonal variations are different, with the values of 60.3 ppm, 36.1 ppm and 29.3 ppm at BJ, XH and XL, respectively. For the diurnal variation, the CO_2 is relatively low during the day and high at night. The diurnal variation of CO_2 at BJ, XH and XL is affected by the BLH, photosynthesis and human activities, and the impact of photosynthesis is more significant at XL.

The CO_2 measurements are compared against the local wind data at BJ and XL. At BJ, high CO_2 mole fractions are observed with low wind speeds (< 2 m.s^{-1}). At XL, the high CO_2 mole fractions during daytime are observed with the wind coming from the south, where the urban area is located.

The two-levels measurements at BJ and XH show that the CO_2 mole fractions at lower and upper levels are close to each other during the day. The CO_2 mole fraction at the lower level is larger than that at the upper level at night with a vertical gradient up to 0.6 ppm/m at XH and 0.2 ppb/m at BJ. There is no clear difference in the CO_2 mole fraction between weekdays and weekends at BJ, XH and XL.

Author contributions. MZ, TW, PW and GW desigend the experiment. YY performed the data curation. YY and MZ wrote the manuscript, and all authors read and provided comments on the paper.

Competing interests. The authors declare that they have no conflict of interest.

https://doi.org/10.5194/acp-2021-103
Preprint. Discussion started: 11 March 2021

Atmospheric Chemistry and Physics Discussions

References

Bagley, J., Rosenthal, D. M., Ruiz-Vera, U. M., Siebers, M. H., Kumar, P., Ort, D. R., and Bernacchi, C. J.: The influence of photosynthetic acclimation to rising CO2 and warmer temperatures on leaf and canopy photosynthesis models, Global Biogeochem. Cycles, 29, 194–206, https://doi.org/10.1002/2014GB004848, 2015.

Bakwin, P. S., Tans, P. P., Hurst, D. F., and Zhao, C.: Measurements of carbon dioxide on very tall towers: results of the NOAA/CMDL program, Tellus B, 50, 401–415, https://doi.org/10.1034/j.1600-0889.1998.t01-4-00001.x, 1998.

Briber, B. M., Hutyra, L. R., Dunn, A. L., Raciti, S. M., and Munger, J. W.: Variations in Atmospheric CO 2 Mixing Ratios across a Boston, MA Urban to Rural Gradient, Land, 2, 304–327, https://doi.org/10.3390/land2030304, 2013.

Chan, D., Ishizawa, M., Higuchi, K., Maksyutov, S., and Chen, J.: Seasonal CO_2 rectifier effect and large-scale extratropical atmospheric transport, J. Geophys. Res. Atmos., 113, https://doi.org/10.1029/2007JD009443, 2008.

Cheng, X. L., Liu, X. M., Liu, Y. J., and Hu, F.: Characteristics of CO_2 Concentration and Flux in the Beijing Urban Area, J. Geophys. Res. Atmos., 123, 1785–1801, https://doi.org/10.1002/2017JD027409, 2018.

Churkina, G.: The role of urbanization in the global carbon cycle., Front. Ecol. Evol., 3, https://doi.org/10.3389/fevo.2015.00144., 2016.

Crippa, M., Oreggioni, G., Guizzardi, D., Muntean, M., Schaaf, E., Vullo, E. L., Solazzo, E., Monforti-Ferrario, F., Olivier, J., and Vignati, E.: Fossil CO_2 and GHG emissions of all world countries - 2019 Report, Publications Office of the European Union, Luxembourg, pp. ISBN 978–92–76–11 100–9, https://doi.org/10.2760/687800, 2019.

Culf, A., Fisch, G., Malhi, Y., and Nobre, C.: The influence of the atmospheric boundary layer on carbon dioxide concentrations over a tropical forest, Agric. For. Meteorol., 85, 149 – 158, https://doi.org/10.1016/S0168-1923(96)02412-4, 1997.

Denning, A. S., Takahashi, T., and Friedlingstein, P.: Can a strong atmospheric CO_2 rectifier effect be reconciled with a "reasonable" carbon budget?, Tellus B, 51, 249–253, https://doi.org/10.1034/j.1600-0889.1999.t01-1-00010.x, 1999.

Dhakal, S.: Urban energy use and carbon emissions from cities in China and policy implications, Energ. Policy., 37, 4208–4219, https://doi.org/10.1016/j.enpol.2009.05.020, 2009.

Fang, S. X., Zhou, L. X., Tans, P. P., Ciais, P., Steinbacher, M., Xu, L., and Luan, T.: In situ measurement of atmospheric CO_2 at the four WMO/GAW stations in China, Atmos. Chem. Phys., 14, 2541–2554, https://doi.org/10.5194/acp-14-2541-2014, 2014.

Feng, T., Zhou, W., Wu, S., Niu, Z., Cheng, P., Xiong, X., and Li, G.: High-resolution simulation of wintertime fossil fuel CO_2 in Beijing, China: Characteristics, sources, and regional transport, Atmos. Environ., 198, 226–235, https://doi.org/10.1016/j.atmosenv.2018.10.054, 2019.

Gao, Y., Lee, X., Liu, S., Hu, N., Wei, X., Hu, C., Liu, C., Zhang, Z., and Yang, Y.: Spatio-temporal variability of the near-surface CO_2 concentration across an industrial-urban-rural transect, Nanjing, China, Sci. Total Environ., 631-632, 1192–1200, https://doi.org/10.1016/j.scitotenv.2018.03.126, 2018.

George, K., Ziska, L., Bunce, J., and Quebedeaux, B.: Elevated atmospheric CO_2 concentration and temperature across an urban-rural transect, Atmo. Environ., 41, 7654–7665, https://doi.org/10.1016/j.atmosenv.2007.08.018, 2007.

Hansen, J., Sato, M., Kharecha, P., and von Schuckmann, K.: Earth's energy imbalance and implications, Atmos. Chem. Phys., 11, 13 421–13 449, https://doi.org/10.5194/acp-11-13421-2011, 2011.

Hernández-Paniagua, I. Y., Lowry, D., Clemitshaw, K. C., Fisher, R. E., France, J. L., Lanoisellé, M., Ramonet, M., and Nisbet, E. G.: Diurnal, seasonal, and annual trends in atmospheric CO2 at southwest London during 2000–2012: Wind sector analysis and comparison with Mace Head, Ireland, Atmos. Environ., 105, 138 – 147, https://doi.org/10.1016/j.atmosenv.2015.01.021, 2015.

https://doi.org/10.5194/acp-2021-103
Preprint. Discussion started: 11 March 2021

Atmospheric Chemistry and Physics Discussions

Hersbach, H., Bell, B., Berrisford, P., Hirahara, S., Horányi, A., Muñoz-Sabater, J., Nicolas, J., Peubey, C., Radu, R., Schepers, D., Simmons, A., Soci, C., Abdalla, S., Abellan, X., Balsamo, G., Bechtold, P., Biavati, G., Bidlot, J., Bonavita, M., De Chiara, G., Dahlgren, P., Dee, D., Diamantakis, M., Dragani, R., Flemming, J., Forbes, R., Fuentes, M., Geer, A., Haimberger, L., Healy, S., Hogan, R. J., Hólm, E., Janisková, M., Keeley, S., Laloyaux, P., Lopez, P., Lupu, C., Radnoti, G., de Rosnay, P., Rozum, I., Vamborg, F., Villaume, S., and Thépaut, J.-N.: The ERA5 global reanalysis, Q. J. R. Meteorol. Soc., 146, 1999–2049, https://doi.org/10.1002/qj.3803, 2020.

Idso, C., Idso, S., and Balling, R.: The urban CO_2 dome of Phoenix, Arizona, Phys. Geogr., 19, 95–108, https://doi.org/10.1080/02723646.1998.10642642, 2013.

IPCC: Climate change 2013: The physical science basis, Contribution of Working Group I to the Fifth Assessment Report of the Intergovernmental Panel on Climate Change, https://www.ipcc.ch/report/ar5/wg1/, 2013.

Kumar, M. K. and Nagendra, S. M. S.: Characteristics of ground level CO2 concentrations over contrasting land uses in a tropical urban environment, Atmos. Environ., 115, 286–294, https://doi.org/10.1016/j.atmosenv.2015.05.044, 2015.

Lac, C., Donnelly, R. P., Masson, V., Pal, S., Riette, S., Donier, S., Queguiner, S., Tanguy, G., Ammoura, L., and Xueref-Remy, I.: CO_2 dispersion modelling over Paris region within the CO_2-MEGAPARIS project, Atmos. Chem. Phys., 13, 4941–4961, https://doi.org/10.5194/acp-13-4941-2013, 2013.

Li, Y., Deng, J., Mu, C., Xing, Z., and Du, K.: Vertical distribution of CO2 in the atmospheric boundary layer: Characteristics and impact of meteorological variables, Atmos. Environ., 91, 110 – 117, https://doi.org/10.1016/j.atmosenv.2014.03.067, 2014.

Liu, H. Z., Feng, J. W., Järvi, L., and Vesala, T.: Four-year (2006–2009) eddy covariance measurements of CO_2 flux over an urban area in Beijing, Atmos. Chem. Phys., 12, 7881–7892, https://doi.org/10.5194/acp-12-7881-2012, 2012.

Lv, Z., Shi, Y., Zang, S., and Sun, L.: Spatial and Temporal Variations of Atmospheric CO2 Concentration in China and Its Influencing Factors, Atmos., 11, 231, https://doi.org/10.3390/atmos11030231, 2020.

Nevison, C. D., Mahowald, N. M., Doney, S. C., Lima, I. D., Werf, G. R. V. D., Randerson, J. T., Baker, D. F., And, P. K., and Mckinley, G. A.: Contribution of ocean, fossil fuel, land biosphere, and biomass burning carbon fluxes to seasonal and interannual variability in atmospheric CO_2, J. Geophys. Res. Biogeo., 113, https://doi.org/10.1029/2007JG000408, 2008.

ángeles García, M., Sánchez, M. L., and Pérez, I. A.: Differences between carbon dioxide levels over suburban and rural sites in Northern Spain, Environ. Sci. Pollut. Res., 19, 432–439, https://doi.org/10.1007/s11356-011-0575-4, 2012.

Shi, Y., Xi, Z., Simayi, M., Li, J., and Xie, S.: Scattered coal is the largest source of ambient volatile organic compounds during the heating season in Beijing, Atmos. Chem. Phys., 20, 9351–9369, https://doi.org/10.5194/acp-20-9351-2020, 2020.

Soegaard, H. and Møller-Jensen, L.: Towards a spatial CO_2 budget of a metropolitan region based on textural image classification and flux measurements, Remote Sens. Environ., 87, 283–294, https://doi.org/10.1016/S0034-4257(03)00185-8, 2003.

Song, T., Wang, Y., and Sun, Y.: Estimation of carbon dioxide flux and source partitioning over Beijing, China, J. Environ. Sci., 25, 2429–2434, https://doi.org/10.1016/S1001-0742(12)60336-2, 2013.

Turnbull, J. C., Sweeney, C., Karion, A., Newberger, T., Lehman, S. J., Tans, P. P., Davis, K. J., Lauvaux, T., Miles, N. L., Richardson, S. J., Cambaliza, M. O., Shepson, P. B., Gurney, K., Patarasuk, R., and Razlivanov, I.: Toward quantification and source sector identification of fossil fuel CO2 emissions from an urban area: Results from the INFLUX experiment, J. Geophys. Res. Atmos., 120, 292–312, https://doi.org/10.1002/2014JD022555, 2015.

Wu, Y., Wang, R., Zhou, Y., Lin, B., Fu, L., He, K., and Hao, J.: On-Road Vehicle Emission Control in Beijing: Past, Present, and Future, Environ. Sci. Technol., 45, 147–153, https://doi.org/10.1021/es1014289, 2011.